Article

Topology Specific Stabilization of Promoter over Telomeric G-Quadruplex DNAs by Bisbenzimidazole Carboxamide Derivatives

V Dhamodharan, S Harikrishna, Achikanath C. Bhasikuttan, and P.I. Pradeepkumar

ACS Chem. Biol., **Just Accepted Manuscript** • DOI: 10.1021/cb5008597 • Publication Date (Web): 11 Dec 2014

Topology Specific Stabilization of Promoter over Telomeric G-Quadruplex DNAs by Bisbenzimidazole Carboxamide Derivatives

V. Dhamodharan,*[‡] S. Harikrishna,[‡] Achikanath C. Bhasikuttan,[§] P. I. Pradeepkumar*[,‡]

[‡]Department of Chemistry, Indian Institute of Technology Bombay, Powai, Mumbai 400076, India

[§]Radiation & Photochemistry Division, Bhabha Atomic Research Centre, Mumbai 400 085, India

E-mail: dhamodharan@chem.iitb.ac.in or pradeep@chem.iitb.ac.in

ABSTRACT

Various potential G-quadruplex forming sequences present in the genome offer a platform to modulate their function by means of stabilizing molecules. Though G-quadruplex structures exhibit diverse structural topologies, the presence of G-quartets as a common structural element makes the design of topology specific ligands a daunting task. To address this, the subtle structural variations of loops and grooves present in the quadruplex structures can be exploited. To this end, we report the design and synthesis of quadruplex stabilizing agents based on bisbenzimidazole carboxamide derivatives of pyridine, 1, 8-naphthyridine and 1, 10-phenanthroline. The designed ligands specifically bind to and stabilize promoter quadruplexes having parallel topology over any of the human telomeric quadruplex topologies (parallel, hybrid or antiparallel) and duplex DNAs. CD melting studies indicate that ligands could impart higher stabilization to *c-MYC* and *c-KIT* promoter quadruplexes (upto 21 °C increment in T_m) than telomeric and duplex DNAs ($\Delta T_m \leq 2.5$ °C). Consistent with CD melting study, ligands bind strongly (K_b = ~10^4-10^5 M^{-1}) to *c-MYC* quadruplex DNA. Molecular modeling and dynamics studies provide insights into how the specificity is achieved, and underscore the importance of flexible *N*-alkyl side chains attached to the benzimidazole-scaffold in recognizing propeller loops of promoter quadruplexes. Overall, the results reported here demonstrate that the benzimidazole scaffold represents a potent and powerful side chain, which could judiciously be assembled with a suitable central core to achieve specific binding to a particular quadruplex topology.

Introduction

G-quadruplexes are structurally diverse and dynamic four stranded nucleic acids formed by stacking of two or more G-quartets in the presence of appropriate metal ions.[1, 2] Number of such putative G-quadruplex-forming sequences in the human genome was estimated to be over 370,000, which will increase further by considering bulge formations in the strands of quadruplexes.[3,4] These quadruplex structures have been detected at the telomere, across the chromosomes and in the transcriptome of the human cells by employing quadruplex-specific antibody and thus validate their existence *in vivo*.[5,6,7] Formation of stable G-quadruplexes induce various effect on cellular functions such as stalling replication,[8] halting function of telomerase enzymes[9] and modulating gene expression at transcription[10] and translation level.[11, 12] Therefore, quadruplexes are harnessed as potential therapeutic targets by exogenous small molecules or ligands.[13] In this direction, small molecules are shown to bind and stabilize the quadruplex structures present in the genome and transcriptome in cellular systems.[5,6] They are also known to induce DNA damage response pathway[14, 15] and promote synthetic lethality in cancer cells.[16]

Various promoter quadruplexes present at the upstream of proto-oncogenes represent the six hallmarks of cancer,[17] and can be targeted by ligands to down-regulate their expression.[10, 18] Most of the promoter quadruplexes such as *c-MYC*,[19] *c-KIT*,[20, 21] *VEGF*,[22] *RET*,[23] *HIF-1α*[24] etc. are known to adopt parallel topology. Contrarily, a growing number of evidences indicate that the parallel form of telomeric DNA might not be biologically relevant target as it requires dehydrated conditions to exist.[25-27] Recent findings suggest that hybrid-1, hybrid-2 and 2-tetrads antiparallel basket topologies are the biologically relevant quadruplex structures for the telomeric DNA.[26, 28-30] Major folding differences between parallel- promoter quadruplexes and telomeric quadruplexes can be exploited for the design of topology-specific ligands. G-quadruplex ligands,

which can specifically discriminate one quadruplex over other quadruplexes without compromising selectivity over duplex, are highly desirable to study structure-specific therapeutic interventions at the genomic level. However, in purely therapeutic point of view, the extent of specificity needed between various quadruplexes is poorly understood. G-quadruplex specific ligand could also be added judiciously along with the quadruplex specific-antibodies to reinforce the visualization quadruplex structure at the precise location in the genome, as reported for the RNA quadruplex visualization by carboxypyridostatin (carboxyPDS) ligand.[6]

Till date, numerous ligands have been reported as G-quadruplex stabilizing agents with high selectivity toward quadruplex over duplex DNAs.[31-33] Nevertheless, it is highly challenging to design a ligand which is specific for targeted quadruplex over other quadruplexes, as G-quartet is the common structural feature in all quadruplexes. But loops (diagonal, lateral, and propeller) and width of the grooves (narrow, medium and wide) are differed for each quadruplex considerably.[34] Furthermore, there are considerable differences in the structures reported for native quadruplexes (without ligand) and quadruplex-ligand complexes as ligand-induced binding pockets are created in the later due to rearrangement of the flexible loops or flanking nucleotides.[35, 36] Therefore, these flexible loops and unique groove widths[34] need to be considered along with the large π surface area of quartet for achieving specific binding of small molecule to the targeted quadruplex topology.[36, 37] Interestingly, few ligands are reported to specifically stabilize human telomeric quadruplex having parallel, antiparallel or hybrid topologies over promoter quadruplexes with parallel topologies. For example, acridine based ligands bind specifically to telomeric DNA over promoter quadruplexes (*c-KIT1, c-KIT2*).[38] Receptor-based virtual screening strategies also identified specific telomeric binding ligands.[39] In addition, ligands which discriminate between various telomeric quadruplexes are also reported.

Oxazole-based heptacyclic derivative (TOxaPy) is able to specifically stabilize antiparallel form of human telomeric DNA over other topologies;[40] *N*-methyl mesoporphyrin IX (NMM) showed specificity for parallel topology over antiparallel topology of telomeric DNA.[41] Recently reported pyridostatin based ligand is able to discriminate telomeric RNA quadruplex from its DNA counterpart.[42]

Ligands having few fold binding preferences for promoter quadruplexes over telomeric DNA are also reported.[43-47] So far, to the best of our knowledge, there is no report on ligands, which specifically bind to and stabilize the promoter quadruplex DNAs over all the known topologies of human telomeric DNA. Moreover, due to lack of structural information, the reasons for the limited topological bias of the reported ligands are poorly understood.

In this work, we report the specific recognition and stabilization of promoter quadruplexes over telomeric quadruplexes by benzimidazole carboxamide derivatives of pyridine, 1, 8-naphthyridine and 1, 10-phenanthroloine (Figure 1). Ligand-induced stabilization of quadruplex and duplex DNAs assessed by CD melting studies show that all ligands are able to impart higher stabilization to promoter quadruplexes (*c-MYC*, *c-KIT1* and *c-KIT2*) over human telomeric and duplex DNAs. CD and NMR titration studies point out that ligand binds to *c-MYC* quadruplex through end-stacking and is able to induce the formation of *c-MYC* quadruplex in the absence of added metal ions. UV-vis titration studies reveal that the ligands could specifically bind to *c-MYC* quadruplex over telomeric and duplex DNA. In addition, the above ligands are able to arrest primer extension at *c-MYC* quadruplex forming site with low IC_{50} values. Structural insights obtained by molecular modeling and dynamics studies explain why ligands bind specifically to parallel quadruplexes over telomeric and duplex DNAs.

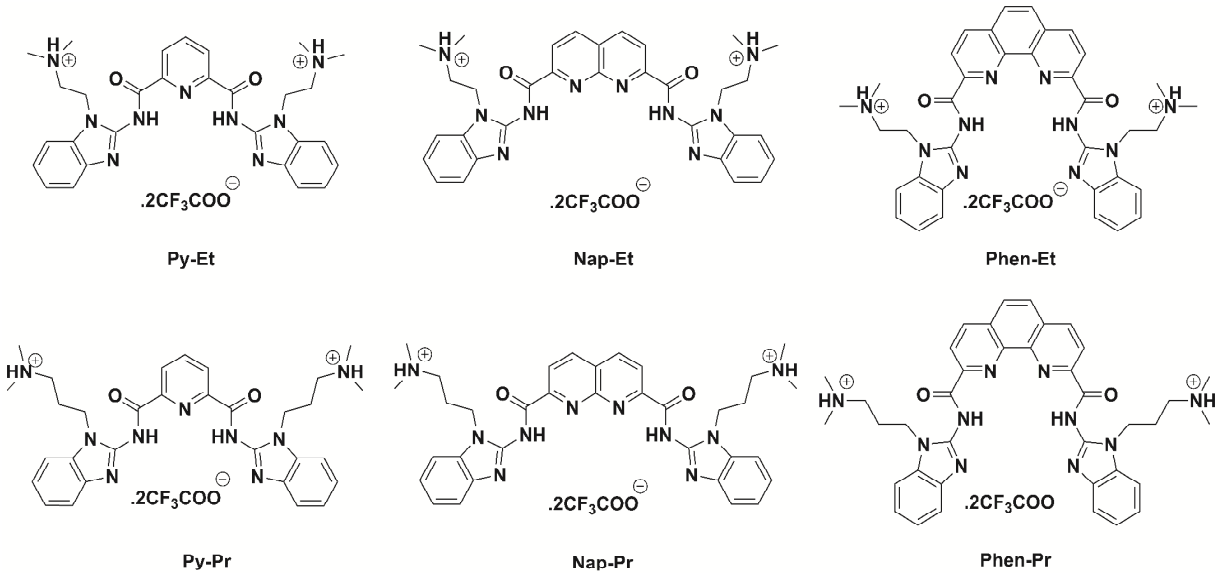

Figure 1. Structures of topology specific G-quadruplex DNA stabilizing ligands. Central cores contain pyridine (Py), 1,8-naphthyridine (Nap) and 1,10 Phenanthroline (Phen) and benzimidazole contains dimethyl aminopropyl (Pr) and dimethyl aminoethyl (Et) as side chains.

RESULTS AND DISCUSSION

Ligand design and synthesis

Benzimidazole scaffolds, which are structural isosteres of purine bases, have widely been studied as duplex groove binders as well as quadruplex DNA stabilizing agents.[48-50] Metal complexes such as platinum (II) and palladium (II) of bisbenzimidazole were able to bind and stabilize quadruplex DNA selectively over duplex DNA.[51, 52] By and large, these benzimidazole based ligands do not discriminate one quadruplex topology over others; and their selectivity was explored only in the context of targeted quadruplex over duplex DNA.[51, 53] Mostly flexible alkyl side chains appended to these benzimidazole ligands are positioned on benzene ring of the benzimidazole moiety.[49, 53] We envisage that the precise location of side chains on imidazole ring of benzimidazole moiety (Figure 1) with appropriate length will have crucial role in differentiating various quadruplexes as accessibility to phosphate backbone of loops of each quadruplex structure is quite different. Herein, six bisbenzimidazole carboxamide derivatives of pyridine, 1,8-naphthyridine and 1,10-phenanthroline were designed and synthesized to

discriminate various quadruplex topologies (Figure 1). The aromatic central cores were chosen because of their presence in several G-quadruplex DNA stabilizing agents.[54-58] The rationales for the design of such ligands are as follows: (1) Nitrogen atoms present in the central core and NH of amide bond can form internal H-bonding, which would fix the ligand conformation to crescent shape.[59] This is expected to enhance its accessibility to the top of the G-quartets. (2) As the benzimidazole scaffold is structurally similar to purine bases, the stacking interactions between benzimidazole and guanine bases in the quartet are anticipated. (3) Furthermore, the positively charged flexible alkyl side chains have the potential to interact with negatively charged phosphate groups present in the loop and grooves.

Syntheses of target molecules (Figure 1) were achieved by coupling corresponding dimethlyaminoethyl or dimethylaminopropyl substituted 2-aminobenzimidazole compounds with appropriate dicarboxylic acid as shown in **Scheme 1**. The key precursors **1** and **2**, needed for the

Scheme 1. Synthesis of bisbenzimidazole derivatives of pyridine, 1,8-naphthyridine and 1,10-phenanthroline carboxamide[a]

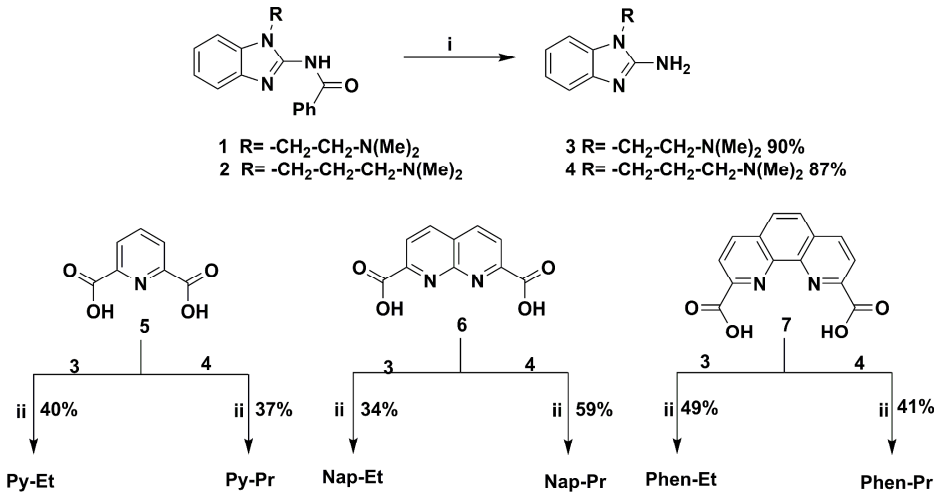

[a]Reagents and conditions: (i) CH_3NH_2-EtOH (33 %), 80 °C, 4 d; (ii) (a) EDC.HCl, HOBt, N-methyl morpholine, DCM, rt, 24 h (b) TFA, DCM, rt, 10 min.

synthesis of side chains **3** and **4**, were prepared using the reported procedures with slight modifications starting from 2-nitrofluorobenzene in 4 steps (Scheme S1, Supporting

information).[60] Deprotection of benzoyl group in **1** and **2** using ethanolic methylamine (~33%) in a sealed tube at 80 °C, furnished the required amine **3** and **4** in 87-90% yields. The direct coupling of these amine compounds **3** and **4** with dicarboxylic acid of pyridine **5**, 1, 8-naphthyridine **6** and 1,10-phenanthroline **7** by EDC.HCl yielded corresponding amide compounds. These amides were treated with trifluoroacetic acid (TFA) to give final ligands **Py-Et**, **Py-Pr**, **Nap-Et**, **Nap-Pr**, **Phen-Et** and **Phen-Pr**, (Figure 1 and Scheme 1) in the protonated forms in 34- 59% yields.

CD melting studies

Initial screening of all ligands (Figure 1) was carried out by CD melting assay, which provided the ligand-induced thermal stabilization of quadruplex and duplex DNAs. Initially, the effect of ligands on human telomeric DNA was tested. Thermal melting of telomeric DNA was monitored at 292 nm since its CD spectrum in K^+ solution has major positive band centered at 292 nm for the mixed populations of parallel and hybrid structures. In the absence of any ligand, the telomeric DNA showed a T_m of 52.6 ± 0.2 °C (Figure 2A, Table 1). In the presence of various ligands the T_m was increased only marginally upto maximum of 2.5 °C. These results clearly point out that ligand-induced stabilization of telomeric DNA is very low. Next we were interested to check the effect of ligands on stabilization of promoter quadruplex DNAs (*c-KIT1*, *c-KIT2* and *c-MYC*). Promoter quadruplexes are known to adopt parallel topology under K^+ condition thus melting study was monitored at 262 nm (Figure 2B and Figure S1, Supporting information). Interestingly, unlike the marginal ligand-induced stabilization observed for telomeric DNA, stabilization of promoter quadruplex was increased upto 20.7 °C for **Phen-Pr** (Table 1). The ΔT_m values are in the range of 1.8 - 10.0 °C for **Py-Et** and **Py-Pr**; 8.1 - 17.8 °C for **Nap-Et** and **Nap-Pr**; 16.0 - 20.7 °C for **Phen-Et** and **Phen-Pr** ligands. This clearly indicates that the effect of stabilization increases with increasing π surface area of the central

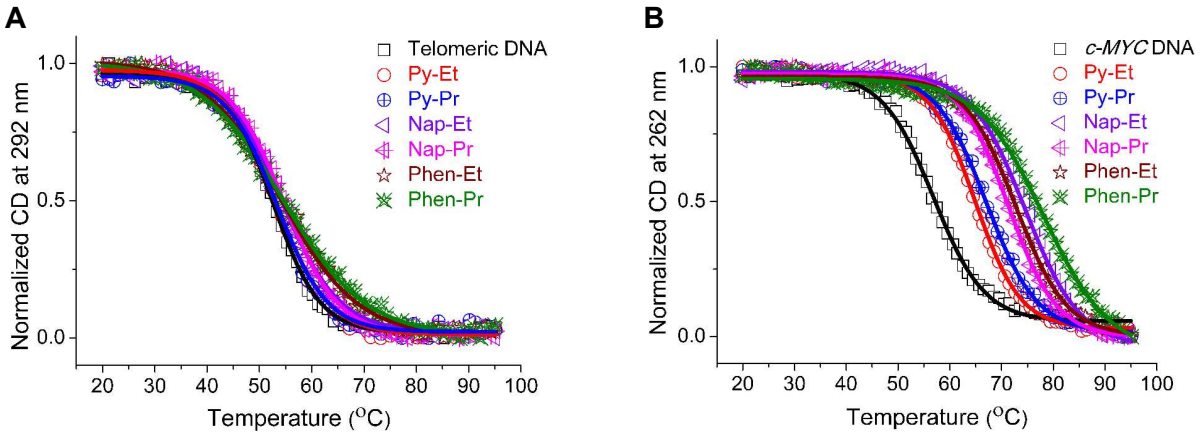

Figure 2. CD melting curves for telomeric and *c-MYC* DNAs (10 µM in 10 mM lithium cacodylate buffer pH 7.2) in the absence and presence of ligands (3 molar eq.). (A) Telomeric DNA (10 mM KCl, and 90 mM LiCl) (B) *c-MYC* DNA (1 mM KCl and 99 mM LiCl).

Table 1. Thermal stability of various quadruplex DNAs and duplex DNA with ligands measured by CD melting experiments

Ligands	ΔT_m [a]				
	Telomeric DNA	*c-KIT1*	*c-KIT2*	*c-MYC*	Duplex ds17
Py-Et	0.5 ± 0.4	7.1 ± 0.3	1.8 ± 0.8	8.0 ± 0.3	1.0 ± 0.4
Py-Pr	0.6 ± 0.2	7.5 ± 0.3	3.7 ± 0.7	10 ± 0.4	2.0 ± 0.4
Nap-Et	1.5 ± 0.5	11.3 ± 0.3	10.3 ± 0.9	17.8 ± 0.2	0
Nap-Pr	2.5 ± 0.5	14.5 ± 0.9	8.1 ± 0.9	14.5 ± 0.8	2.3 ± 0.4
Phen-Et	1.0 ± 0.8	18.5 ± 0.9	16.3 ± 0.6	16.0 ± 0.3	0
Phen-Pr	1.7 ± 0.8	20.7 ± 1.1	16.6 ± 0.7	19.6 ± 0.5	n.d

[a] ΔT_m represents shift in thermal melting [$\Delta T_m = T_m$ (DNA + 3 molar equivalents ligand) − T_m (DNA)]. For all experiments DNA 10 µM for quadruplex or 15 µM for duplex DNA in 10 mM lithium cacodylate buffer pH 7.2 were used. The T_m values are: 52.6 ± 0.2 °C [telomeric DNA in 10 mM KCl, 90 mM LiCl]; 47.7 ± 0.3 °C [*c-KIT1* DNA in 10 mM KCl, 90 mM LiCl]; 52.8 ± 0.6 °C [*c-KIT2* DNA in 1 mM KCl, 99 mM LiCl]; 56.7 ± 0.1 °C [*c-MYC* DNA in 1 mM KCl, 99 mM LiCl]; 62.7 ± 0.4 °C [ds-17 DNA in 10 mM KCl and 90 mM LiCl]. All experiments were triplicated and the values reported are average of three independent measurements with the estimated standard deviation. As the ionic strength is known to modulate the binding of a cationic ligand to the negatively charged DNA, for all melting experiments, a total ionic strength of 110 mM was maintained with the help of Li^+ ions, which does not alter the structure and stability of the K^+-induced quadruplex forms.[61]

core (1,10-phenanthroline> 1,8-naphthyridine > pyridine). However, there is no conclusive order in the magnitude of stabilization of promoter quadruplexes with increasing side chain length from dimethylaminoethyl to dimethylaminopropyl due to the presence of diverse central cores in the ligands. To further validate our findings on the distinct specificity of the ligands toward promoter quadruplexes, melting experiments were also carried out with a well-characterized ligand, **3AQN (**bisquinolium derivative of 1,8-naphthyridine)[55, 58] under the identical salt and buffer conditions. Results showed that the reference compound **3AQN** conferred stability to both telomeric (ΔT_m = 24.0) and *c-MYC* (ΔT_m > 30.0) quadruplex DNAs (Figure S2, Supporting information), contrasting to the results obtained with bisbenzimidazole ligands (Table 1).

Having established specific stabilization promoter quadruplexes over telomeric DNA by the benzimidazole ligands, the ability of ligand to stabilize duplex DNA was also verified. Thermal stability of duplex DNA monitored at 242 nm provided a T_m of 62.7 ± 0.4 °C in the absence of ligands (Table 1, Figure S1C, Supporting Information). The stability of duplex DNA upon addition of ligands was increased by 2.3 °C. Remarkably, there was no detectable stabilization observed for duplex DNA in the presence of **Nap-Et** and **Phen-Et** ligands. Overall results show that ligands selectively stabilize promoter quadruplexes over duplex DNAs.

Since the telomeric DNA is known to adopt antiparallel topology in the presence of Na^+ ions, melting studies were performed to examine whether these ligands could stabilize the antiparallel topology. Due to the lowest induced-stabilization effect of **Phen-Et** to the telomeric DNA (ΔT_m = 1 °C), further studies were focused on this ligand. Thermal melting of antiparallel form of telomeric DNA provided T_m of 51.2 ± 0.4 °C in the absence of ligands (Figure S3A, supporting Information). Addition of **Phen-Et** resulted in no change in T_m, indicating the ligand did not stabilize the antiparallel quadruplex structure of telomeric DNA (Figure S3A, Supporting

Information). Having established marginal ligand-induced stabilization of telomeric quadruplex DNA both in Na^+ and K^+ ions, we evaluated the effect of ligand to the parallel topology of telomeric DNA. It is reported that under polyethylene glycol (PEG) condition in the presence of K^+ ions, telomeric DNA is known to adopt only a parallel topology.[62] Similar to the results obtained with antiparallel quadruplex topology, addition of **Phen-Et** showed no stabilizing effect on the telomeric parallel topology (Figure S3B, Supporting information). In contrast, the reference compound **3AQN** stabilizes the PEG-induced parallel quadruplex DNA by a ΔT_m = 10.0 (Figure S3C, Supporting information), distinguishing it from **Phen-Et**.

Other possibility one should not rule out is the formation of higher-order quadruplex structures by human telomeric DNA.[26, 30, 63] In order to study whether the ligand, **Phen-Et**, can stabilize this higher order form of telomeric DNA, a sequence $AGGG(TTAGGG)_7$, which can form two contiguous quadruplexes, was used. Results show that T_m of long telomeric quadruplex DNA was increased only by ~2 °C in the presence of ligand (Figure S3D, Supporting Information). Overall the CD melting data indicate that ligands are less effective in stabilizing any of the telomeric DNA topological forms (antiprallel, parallel, hybrid or higher order forms). The marginal ligand-assisted stabilization observed for telomeric DNA prompted us to rationalize these findings. Quadruplexes have different sites (quartets, loops and grooves) to which ligands bind via various non-covalent interactions such as stacking, electrostatic, and hydrogen-bonding and van der Waals forces. It appears that parallel form of promoter quadruplexes fulfill the structural requirements to maximize these non-covalent interactions with the ligands. These aspects were probed in details by molecular modeling and dynamics studies (see in respective section).

CD and NMR titration studies

CD studies were performed to examine whether the ligand could induce quadruplex structures from the promoter and telomeric DNAs in the absence of added metal ions. In the absence of added metal ions, *c-MYC* DNA exhibited positive peak at 264 nm and a negative peak at 240 nm (Figure 3A), which are consistent with the parallel topology. Upon addition of **Phen-Et**, the ellipticity at 263 nm remarkably increased, indicating strong induction of quadruplex form (Figure 3A). Other promoter DNAs such as *c-KIT1* and *c-KIT2* were also induced the parallel

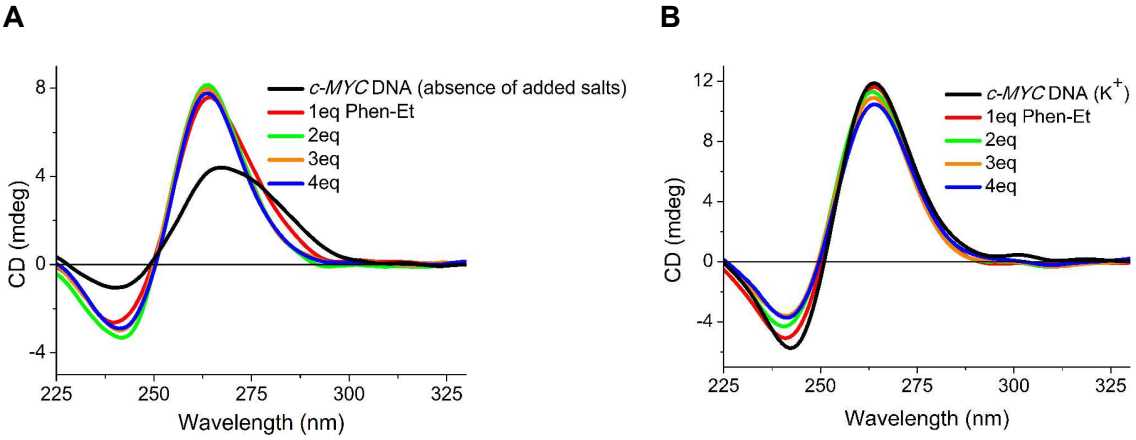

Figure 3. CD titration of ligand **Phen-Et** to *c-MYC* DNA (15 μM in 10 mM Tris buffer pH 7.2) in the presence and absence of K^+ ions. (A) *c-MYC* DNA with increasing molar eq. (0 to 4) of **Phen-Et**. (B) *c-MYC* DNA (100 mM KCl) with increasing molar eq. (0 to 4) of **Phen Et**.

form of quadruplex but with less prominent CD enhancement by the addition of **Phen-Et** (Figure S4A and B, Supporting Information). Contrarily, CD spectrum of telomeric DNA in the absence of added metal ions showed weak positive band at 256 nm and negative bands at 279 and 238 nm (Figure S3C, Supporting Information).[64] In the presence of **Phen-Et**, no well-defined quadruplex peaks corresponding to any of the known topologies were observed (Figure S4C Supporting Information), owing to its non-specific interactions with an unfolded-telomeric DNA structure. In contrast, many classes of G-quadruplex selective ligands such as Telomestatin,[64]

bisquinolinium compounds (**360A**, **3AQN**),[55] and thioflavin T[33] are known to induce antiparallel quadruplex structure of the telomeric DNA in the absence of added salts.

CD studies were also performed in the presence of metal ions (K^+) to examine the structural changes of preformed-quadruplex upon addition of ligand. In the presence of K^+ ions, *c-MYC* DNA exists in parallel form as evidenced from the positive peak at 263 nm and negative peak 242 nm (Figure 3B).[65] Addition of **Phen-Et** to the preformed-quadruplex led to very slight changes in ellipticity and the parallel topology was retained in the folded form. Similarly, parallel topologies of *c-KIT1* and *c-KIT2* quadruplex structures were retained after addition of **Phen-Et** (Figure S5A and B, Supporting Information). In the case of telomeric quadruplex DNA, induction of weak antiparallel form was observed by the addition of ligand (Figure S5C, Supporting Information). However, from the CD melting studies, it was apparent that such induction by the ligand has conferred only marginal stability to the telomeric quadruplex DNA. Overall, CD studies clearly suggest that **Phen-Et** is able to induce and stabilize the parallel quadruplex form of *c-MYC* quadruplex DNA.

Imino-protons in the ^{1}H NMR spectra of quadruplex and quadruplex-ligand complex provide valuable insights into stoichiometry and binding mode of ligands. It is reported that when ligands bind to quadruplex by end-stacking mode, the imino-proton peaks of all G-quartets get shielded, which leads to up-field chemical shifts.[66-68] In contrast, when ligands bind to grooves of quadruplex, chemical shifts of imino protons are unaffected or undergo only nominal changes.[39, 65, 69] NMR spectrum of *c-MYC* DNA showed 12 well-resolved distinct peaks in the imino region corresponding to 12 guanines present in the 3-quartets of quadruplex (Figure 4).[66] However, when 0.5 molar eq. of **Phen-Et** was titrated into *c-MYC* DNA, a new-set of peaks with up-field chemical shifts for ligand-quadruplex complex were emerged, while the peaks

correspond to *c-MYC* DNA (without ligand) were also present (Figure 4). This clearly indicates that ligand favors end- stacking binding mode and, however, a complete saturation of quadruplex was not attained due to which mixed populations of both quadruplex and quadruplex-ligand complex coexisted. Interestingly, upon addition of 1 molar eq. of **Phen-Et** (1:1 stoichiometry), only the up-field shifted imino-protons for a single dominant conformation of quadruplex-ligand complex were observed (Figure 4). These results are in line with recently reported NMR studies of quadruplex-ligand complexes wherein quindoline and phenanthroline-bisquinolinium (Phen-DC3) compounds induce up-field shift of all imino-protons as they bind onto the terminal quartet of *c-MYC* quadruplex. [66, 68]

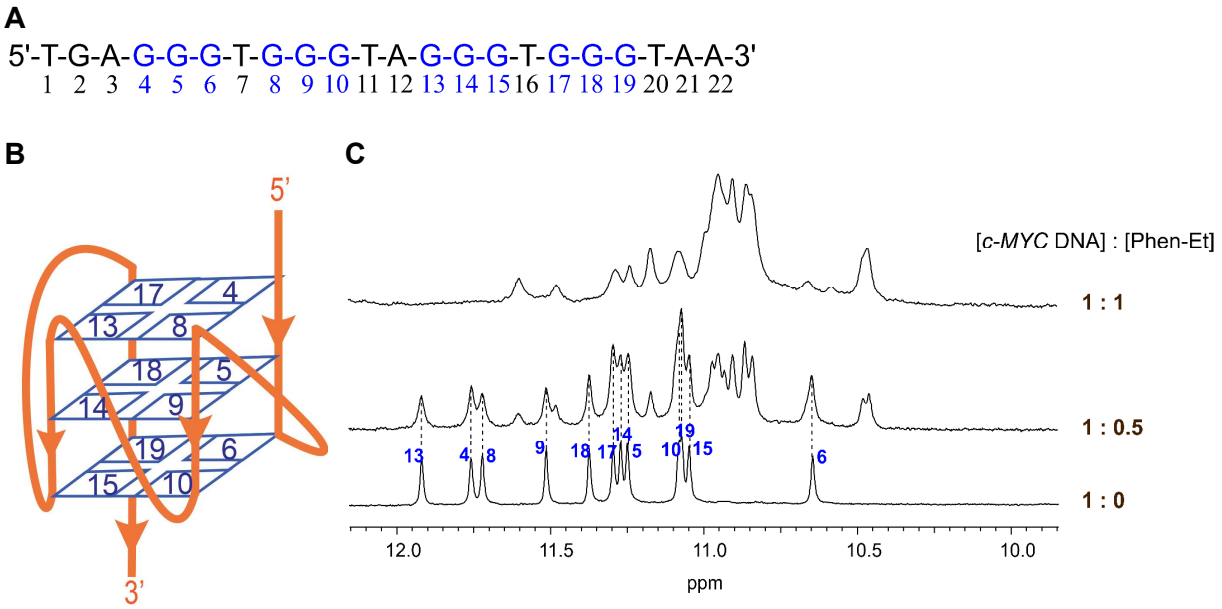

Figure 4. Sequence, topology and ^{1}H NMR (800 MHz) spectra and of *c-MYC* DNA. (A) Sequence of *c-MYC* DNA. The guanine bases (G) which are involved in G-quartet formation are labelled in blue color. (B) Topology of the parallel *c-MYC* quadruplex DNA.[19] (C) ^{1}H NMR spectra of imino region of *c-MYC* DNA (227 µM in 80 mM KCl and 20 mM Potassium phosphate buffer pH 6.7) in the absence and presence of **Phen-Et**. Spectra were recorded in H_2O:D_2O mixture (9:1) at 25 °C. At 1 (DNA): 0.5 (ligand) molar ratio, both *c-MYC* quadruplex-ligand complex and *c-MYC* quadruplex coexist and at 1:1 molar ratio only the quadruplex-ligand complex exists. Dotted lines indicate imino protons corresponding to the ligand-free *c-MYC* quadruplex. Imino protons of G-quartets were labelled based on the previous literature.[19]

UV-Vis absorption studies

UV titration experiments were performed to find binding constant of the ligands with various DNAs. Ligands are known to exhibit bathochromic shift, hyperchromicity or hypochromicity upon binding with DNA.[33, 51, 70, 71] A solution of **Phen-Et** displayed absorbance maxima at 282 nm and around 344 nm (Figure 5A). Addition of *c-MYC* quadruplex to this solution resulted in

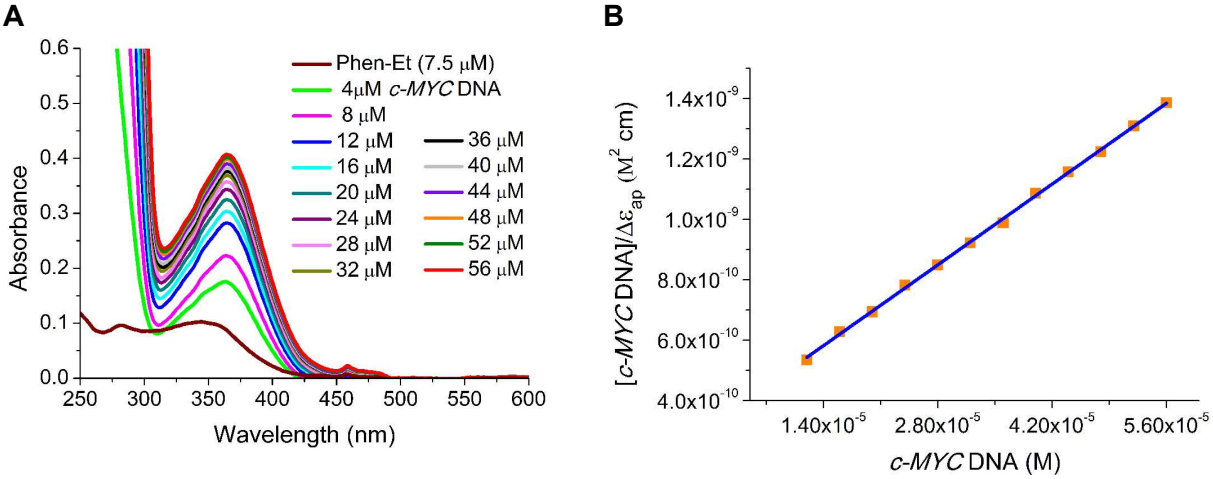

Figure 5. Absorption spectra of **Phen-Et** and with *c-MYC* DNA and the binding plot. (A) Addition of *c-MYC* DNA (4-56 μM in 100 mM KCl and 10 mM lithium cacodylate pH 7.2) into the solution of **Phen-Et** (7.5 μM in the identical salt and buffer conditions) at 25 °C. (B) Plot of [*c-MYC* DNA]/$\Delta\varepsilon_{ap}$ versus [*c-MYC* DNA].

red-shift by 20 nm and remarkable hyperchromicity at 364 nm (Figure 5A), indicating strong interaction of **Phen-Et** and *c-MYC* quadruplex DNA. The ratio of slope-to-intercept, obtained by plotting of [*c-MYC*]/$\Delta\varepsilon_{ap}$ versus [*c-MYC*], provided binding constant (K_b) of (6.39 ± 0.33) x 10^4 M^{-1} at 25 °C (Figure 5B, see experimental section in Supporting information for details). Under identical salt and buffer concentration, UV-Vis titrations were also performed for telomeric and duplex DNA (Figure S6, Supporting Information). Though red-shift was observed upon addition of telomeric and duplex DNA to the **Phen-Et** solution, there was only a slight change in the absorbance at 364 nm (Figure S6, Supporting Information). Due to the very weak interaction of **Phen-Et** with telomeric and duplex DNA, we were not able to deduce the binding constants.

These results clearly reinstate that **Phen-Et** specifically binds to and stabilizes *c-MYC* quadruplex over telomeric and duplex DNAs.

Since **Phen-Pr** has imparted higher stabilization to *c-MYC* quadruplex over other ligands, its binding affinity to *c-MYC* quadruplex was also determined. Consistent with **Phen-Et** ligand, addition of *c-MYC* DNA into the solution of **Phen-Pr** also exhibited red-shift (by 20 nm) and remarkable hyperchromicity at 364 nm. The binding constant (K_b) of **Phen-Pr** was found to be (2.41 ± 0.16) x 10^5 M^{-1}, which is ~4 fold higher than that of **Phen-Et** (Figure S7A and B, Supporting Information). It is apparent that the observed binding affinities of the ligands are moderate and lower than the potent G-quadruplex stabilizing ligands such as Pyridostatin (PDS).[72] This underscore that G-quadruplex specific ligands may not exhibit very high binding affinity so as to maintain the biding specificity confined to a particular topology. Overall, consistent with melting study, the ligands **Phen-Et** and **Phen-Pr** have higher binding affinity and specificity for *c-MYC* quadruplex over telomeric and duplex DNAs (Figure S7C and D, Supporting Information).

***Taq* polymerase stop assay**

Ligand-induced stability of quadruplex DNA was further probed by *Taq* polymerase stop assay.[73,74] Here templates containing *c-MYC* quadruplex forming sequence and non-quadruplex forming sequence (mutated *c-MYC* DNA in which one G was replaced by A) were used. In the absence of ligand at 55 °C, *Taq* polymerase was able to extend the primer into full length product when *c-MYC* quadruplex forming template was used (Figure 6, Figure S8 and S9, Supporting Information). However, in the presence of ligand, quadruplex structure present in the template being stabilized, due to which *Taq* polymerase was unable to unwind this stable

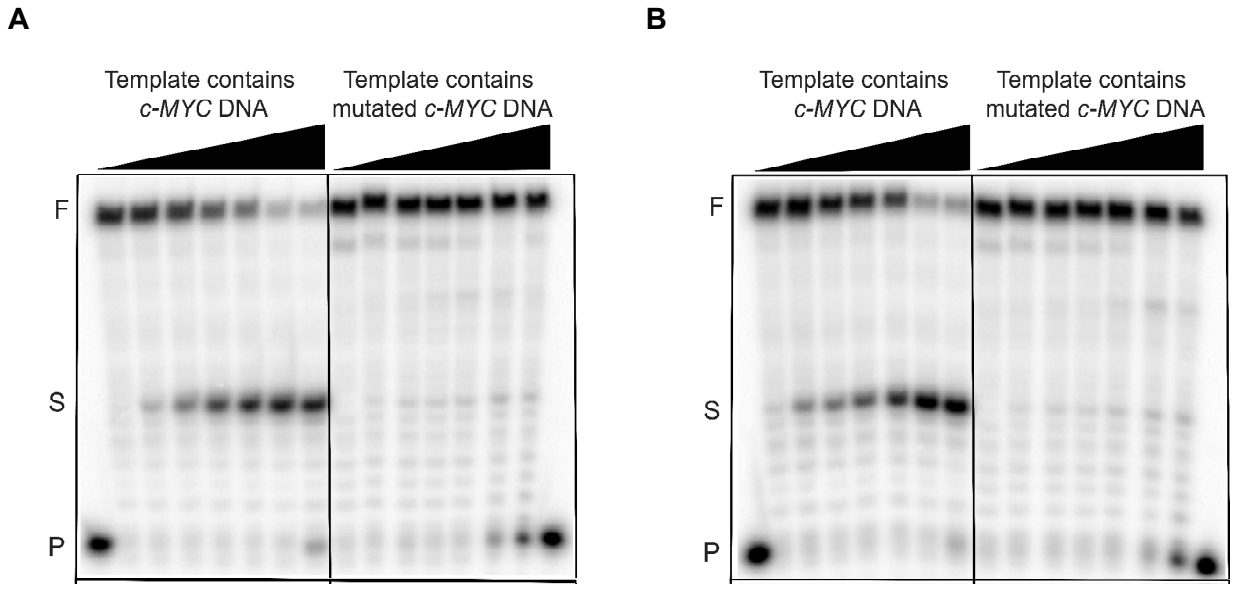

Figure 6. Denaturing PAGE (15%, 7M urea) of primer-extension stop assay by *Taq* polymerase. Template sequence contains quadruplex forming *c-MYC* DNA and non-quadruplex forming mutated *c-MYC* DNA (100 nM template, 50 nM primer, 0.2 mM dNTPs and 0.5 U *Taq* polymerase) (A) **Phen-Et** (0, 0.25, 0.5, 1, 2, 4 and 8 μM). (B) **Phen-Pr** (0, 0.1, 0.2, 0.3, 0.5, 1 and 2 μM). F, S and P denote Full length product, Stop product at quadruplex forming site and Primer respectively. Extension of primer by *Taq* polymerase at 55 °C leads to full length product in the absence of ligand whereas in the presence of ligands, which stabilize the quadruplex, extension is paused at quadruplex forming site.

quadruplex to get full length product. Hence, instead of full length product, there was stop product at the quadruplex forming site in the presence of ligand. Plotting percentage of stop product versus concentration of ligand used furnishes the IC_{50} values (Figure S10, Supporting Information). The ligands **Nap-Et** and **Nap-Pr** showed IC_{50} values of ~ 0.8 μM and ~ 7.2 μM; phenanthroline based ligands, **Phen-Et** and **Phen-Pr**, showed IC_{50} values of ~1.0 μM and ~0.5 μM respectively (Figure S10, Supporting Information). In case of pyridine based ligands, **Py-Et** and **Py-Pr**, full length product was observed even at 100 μM (Figure S9, Supporting Information) due to the poor stabilization of quadruplexes by them. It should be noted that in the case of **Nap-Et**, at high concentration (3 μM), pausing sites were observed not only in the quadruplex forming site but also primer-template site due to its binding to single/ double

stranded DNA (Figure S8A, Supporting Information). Similar results were also observed for the potent ligands such as Telomestatin and Amidoanthroquinone (BSU-1051). [73, 43]

Template sequence containing non-quadruplex forming region (mutated *c-MYC*) was also studied under identical condition to evaluate any non-specific binding of the ligands (Figure 6). Results indicate that all ligands, except **Nap-Et**, showed no effect on the mutated DNA, which further substantiate that inhibition of primer extension is quadruplex mediated and the ligands have higher binding affinity for quadruplex over single and double stranded DNAs. In the case of **Nap-Et**, pausing sites were observed due to its non-specific binding to single or double stranded DNA (Figure S8A, Supporting Information). Overall, the IC_{50} values are well in agreement with CD melting data of *c-MYC* quadruplex DNA, where **Phen-Pr** imparted highest stabilization (ΔT_m = 20.7 °C) and showed lowest IC_{50} value (~ 0.5 μM).

Molecular modeling and dynamics studies

Molecular dynamics (MD) simulation studies were carried out to decipher the structural basis of ligand specificity in binding and stabilizing promoter G-quadruplex over telomeric G-quadruplex and ds DNAs. All the ligands were energy optimized at B3LYP/6-311G** level in Gaussian 09,[75] and optimized geometries showed that conformational freedom of the ligands was strictly restricted by two intra-molecular hydrogen bonds between *N*-atoms in the aromatic core and H atoms in the amide group linking the side chains (Figure S11, Supporting Information). Molecular docking studies were performed using Glide with the energy optimized structures of **Phen-Et** and **Phen-Pr** ligands with *c-MYC* (PDB entry: 1XAV),[19] telomeric parallel (PDB entry: 1KF1),[76] hybrid (PDB entry: 2MB3)[67] and antiparallel (PDB entry: 143D)[77] G-quadruplex structures. All the docked structures showed top G-quartet as the preferred binding site for the ligands. The docked structures were subjected to a 100 ns of unrestrained MD simulations using

AMBER 12 package.[78] Generalized AMBER force field[79] and FF12SB were used for ligand and DNA respectively.

Binding free energies for all G-quadruplex-ligand complexes were estimated using MM-PB/GBSA method.[80] The total binding free energy (ΔG, Table 2, Tables S1-S3, Supporting Information) clearly showed that **Phen-Et** and **Phen-Pr** have higher selectivity/specificity

Table 2. Binding free energy (ΔG, kcal mol^{-1}) for G-quadruplex and ds DNA with each ligand estimated using MM-PB/GBSA in AMBER 12.

Structures	**Phen-Et**	**Phen-Pr**
c-MYC (1XAV)	−61.67 ± 3.4[a]	−66.65 ± 4.2
Telomeric antiparallel (143D)	−35.57 ± 6.7	−42.38 ± 6.7
Telomeric hybrid (2MB3)	−12.13 ± 3.7	−42.28 ± 5.2
dsDNA	−14.47 ± 5.2	−20.00 ± 2.9

[a]Standard deviation of the ΔG values calculated from 100 ns of MD simulations.

toward parallel *c-MYC* quadruplex (~ −61-66 kcal mol^{-1}) over telomeric (~ −12-42 kcal mol^{-1}) and duplex (~ −14-20 kcal mol^{-1}) DNAs. Results also highlight that **Phen-Et** is more specific than **Phen-Pr** towards *c-MYC* over telomeric quadruplex DNA.

It should be noted that there exist major structural differences between *c-MYC* and telomeric quadruplex topologies. The telomeric parallel and *c-MYC* structure contain only propeller loops, whereas telomeric antiparallel structure contains two lateral and one diagonal loop, and hybrid structure contains two lateral and one propeller loop.[19, 67,77] These diverse loop conformations, and their orientation of the sugar phosphate backbone could make differences in the binding sites for G-quadruplex interacting ligands. The MD snapshot for the **Phen-Et** and **Phen-Pr** with *c-MYC* -quadruplex unveiled that G-quartet surface along with the re-oriented 5'-flanking nucleotides create a well-defined binding site (**Figure 7**).[68] As a result, ligands were

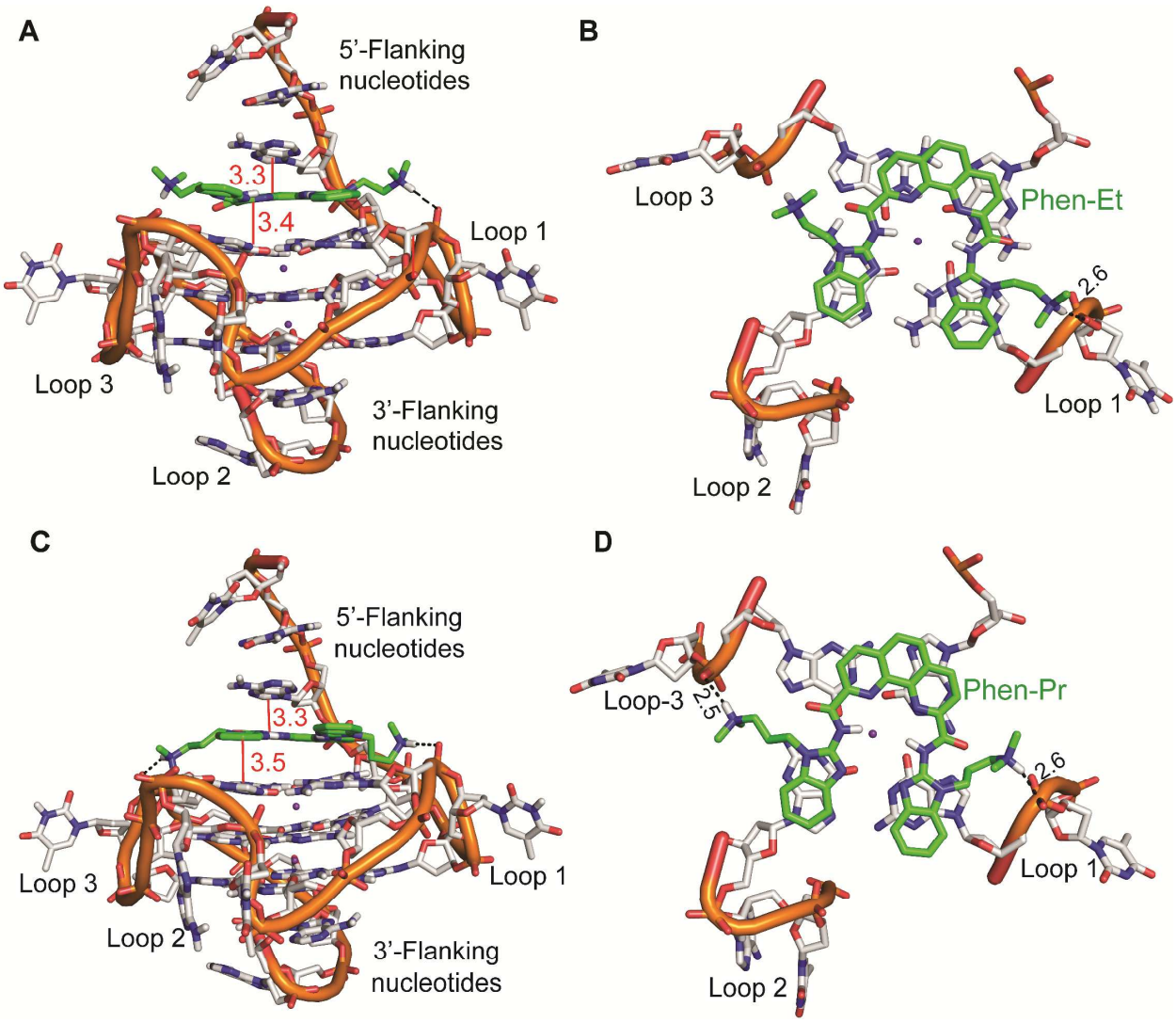

Figure 7. Final MD snapshot of **Phen-Et** and **Phen-Pr** with *c-MYC* G-quadruplex DNA after 100 ns simulations. (A) **Phen-Et** bound to *c-MYC* quadruplex (side view). (B) **Phen-Et** stacks on 5'-quartet and makes electrostatic interactions with the loops (axial view). (C) **Phen-Pr** bound to *c-MYC* quadruplex (side view). (D) **Phen-Pr** stacks on 5'-quartet and makes electrostatic interaction with loops (axial view). The red lines indicate the distance between nucleobases and ligand; black dotted lines denote the electrostatic interactions between ligands and DNA. Phosphate backbone and nucleosides are represented in cartoon and stick representation respectively. The K^+ ions are shown in purple sphere. All the distances are mentioned in Å.

able to stack on top of all the four guanines present in the quartet of *c-MYC* DNA. The MD snapshot of **Phen-Et** with telomeric antiparallel G-quadruplex showed that only central phenanthroline ring stacked on to the G-quartet, while two benzimidazole side chains were away from G-quartet surface (Figure S12, Supporting Information). However, the MD snapshot of telomeric hybrid G-quadruplex DNA and ligands revealed that **Phen-Pr** stacks well on the top of

the G-quartet (Figure S13, Supporting Information). In addition, both ligands in the presence of telomeric antiparallel G-quadruplex DNA underwent energetically unfavorable amide bond rotations during the course of MD simulations (Figure S12, Supporting Information). Interestingly, **Phen-Et** and **Phen-Pr** retained their energy optimized conformation during the course of dynamics, when they bound to *c-MYC* G-quadruplex DNA (Figure S14, Supporting Information). Overall, these results suggest that **Phen-Et**, which has a shorter side chain than **Phen-Pr**, could impart higher specificity towards *c-MYC* G-quadruplex DNA over telomeric G-quadruplex topologies. The differences in binding preference of the ligands toward different topologies imply that intrinsic flexibility of flanking nucleotides in *c-MYC*, which is lacking in telomeric DNA, should be considered for the design of topology specific G-quadruplex stabilizing ligands.[66]

To unveil the link between the length of side chains and observed quadruplex specificity, the distances between the protonated side chains in the ligands and phosphate groups present in the loop of G-quadruplex DNA were probed. One of the ^{N}-protonated side chains of **Phen-Et** and phosphate backbone of propeller loop of *c-MYC* G-quadruplex forms electrostatic interactions as the distance between them was found to be 2.6 ± 0.5 Å (Figure 7C and 7D). Such interaction was not observed in the other protonated side chain of **Phen-Et**. In the case of **Phen-Pr**, both *N*-Protonated side chains were in close contact (~2.6 Å) with phosphate backbone of propeller loops, favoring electrostatic interactions (Figure 7D). Conversely, the distance between the protonated side chains and phosphate group in the diagonal and lateral loop of telomeric G-quadruplex structures was ~ 8.2 Å, deterring **Phen-Et** to form the favorable electrostatic interactions (Figure S15, Supporting Information). Contrarily, one of the *N*-protonated side chains of **Phen-Pr** was located at a distance of ~3.2 Å from negatively charged

phosphate backbone of lateral and diagonal loops present in telomeric quadruplex structures, thus favoring electrostatic interactions (Figure S15, Supporting Information). These results validate that the length of side chains play critical role in discriminating various quadruplex topologies.

To further understand the role of non-covalent interactions of ligand binding to G-quadruplex DNAs, presence of stacking and electrostatic interactions were probed at each pico second (ps) during the course of 100 ns of MD simulations. For electrostatic interactions, distance of ≤ 3.5 Å cutoff was considered between positively charged *N*-protonated side chains of the ligand and the negatively charged DNA backbone. Similarly, for the analysis of stacking interactions, the distance of ≤ 3.5 Å between the ligand and G-quartet was considered along with ± 10° vector angle of the planes. In the case of Phen-**Et** and **Phen-Pr** ligands with *c-MYC* G-quadruplex, both the electrostatic and stacking interactions were found to be present ~85% of the total simulation time (Table S4, Supporting Information). The combined effect of these two non-covalent interactions facilitates the ligands to form a stable complex with *c-MYC* G-quadruplex DNA. Interestingly, **Phen-Et** with telomeric antiparallel quadruplex structure showed that electrostatic and stacking interactions were present only ~45% and ~39% of the simulation time respectively. In case of telomeric hybrid structure, **Phen-Et** maintained only ~8% of stacking and ~6% electrostatic interactions (Table S4, Supporting Information). However, **Phen-Pr** with human telomeric antiparallel and hybrid G-quadruplex showed the presence both of the interactions more than ~50% of simulation time. The low prevalence of these non-covalent interactions between the ligands and telomeric quadruplex topologies accounts for their weak stabilizing effects observed in the experiments. Additionally, energetics of $\pi - \pi$ stacking[81] of quadruplex-ligand complexes were computed at MP2/6-31G* (0.25) level in Gaussian 09 (Table

3 and Table S5, Supporting Information). For the stacking energy calculations, the structures of original G-quadruplex and structure obtained after 100 ns of MD simulation with ligands were utilized. Difference in the stacking energy of the two structures is shown in **Table 3**. The results clearly show that the ligands have better stacking affinity with *c-MYC* G-quadruplex DNA over telomeric DNA topologies. Additionally, stacking energy calculations reveals that **Phen-Et** is more specific toward *c-MYC* quadruplex than **Phen-Pr**.

Table 3. **Difference in the stacking energy of G-quadruplex DNA in the geometry of ligand unbound state and bound state calculated at MP2/6-31G*(0.25) level (kcal mol^{-1}) in Gaussian 09.**

Structures	*c-MYC* G-quadruplex (PDB entry: 1XAV)	Telomeric antiparallel G-quadruplex (PDB entry: 143D)	Telomeric hybrid G-quadruplex (PDB entry: 2MB3)
Phen-Et	–20.80	–3.73	–3.70
Phen-Pr	–22.51	–9.76	–10.89

The conformational stability of the quadruplex-ligand complexes were analyzed using the 1D and 2D RMSD maps. The RMSD analysis of G-quartets and ligands showed all atoms were within 1.5 Å during the course of 100 ns MD simulations in quadruplex-ligand complexes (Figure S16-S18, Supporting Information). The 5'-flanking nucleotides (RMSD = 2.8 ± 0.5 Å) in *c-MYC* G-quadruplex underwent a global conformational change to accommodate the ligands in such a way as to maximize their interactions with G-quartets (Table S6, Supporting Information). Contrarily, the 3'-flanking tri-nucleotides (RMSD = 1.8 ± 0.3 Å) of *c-MYC* quadruplex stacked rigidly to the bottom of G-quartet. The ligand **Phen-Et** did not form a rigid complex with telomeric hybrid G-quadruplex as evidenced from higher RMSD of lateral loop (RMSD = 2.4 ± 0.8 Å) and ligand (RMSD = 3.1 ± 0.4 Å). Such deviations were not observed for **Phen-Pr** and telomeric hybrid G-quadruplex DNA (Table S6, Supporting Information). Furthermore, the two

dimensional RMSD maps of quadruplex-ligand complexes validate the conformational flexibility of **Phen-Et** with telomeric quadruplex structures during the course of MD simulations (Figure S19-S21, Supporting Information).

It has been reported that binding preference of a ligand to a particular G-quadruplex topology or structure depends on its ability to maximize the available accessible surface area in the receptor quadruplex structure.[82] To delineate this aspect, solvent accessible surface area (SASA) of the quadruplex over the 100 ns of MD simulation was calculated for the quadruplex-ligand complexes using Surf tool in AMBER 12. The normalized frequency of SASA during the course of simulation was analyzed (Figure S22, Supporting Information). The **Phen-Et** and **Phen-Pr** accessed large surface area of *c-MYC* G-quadruplex with ΔSASA of 238 Å^2 and 253 Å^2 respectively (Figure 8). However for the **Phen-Et,** ΔSASAs with telomeric antiparallel and

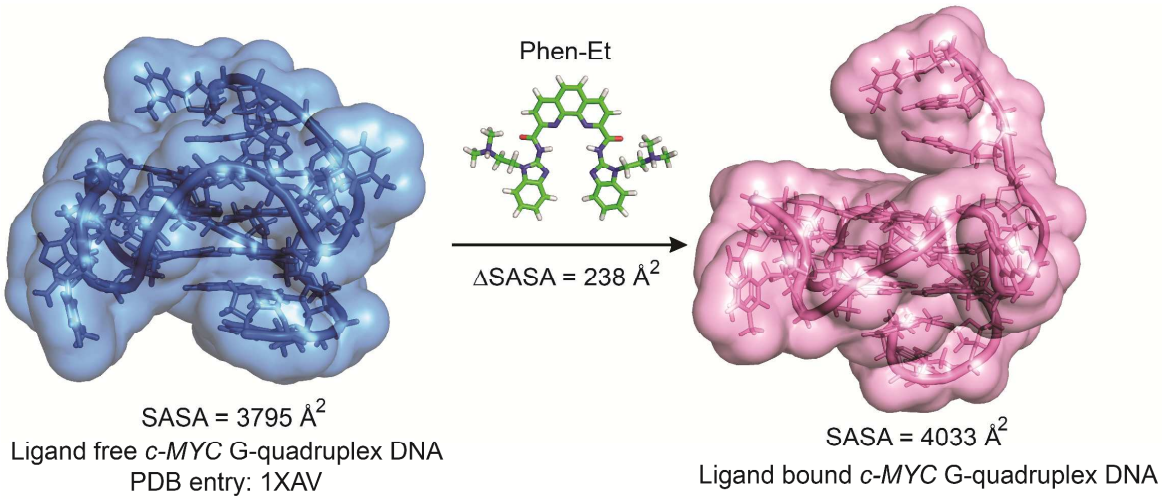

Figure 8. Comparison of solvent accessible surface area (SASA) between native and **Phen-Et** bound *c-MYC* quadruplex DNAs. ΔSASA = (SASA of **Phen-Et** bound *c-MYC* quadruplex complex) – (SASA of native *c-MYC* quadruplex DNA). SASA of **Phen-Et** bound *c-MYC* complex was calculated after 100 ns of MD simulations.

hybrid were found to be only 173 Å^2 and 169 Å^2 respectively. The difference in the ΔSASA between parallel *c-MYC* and telomeric G-quadruplex topology is around 60 Å^2, therefore the ligands favor *c-MYC* G-quadruplex over telomeric DNA topologies. The ability of ligand in

accessing the surface area of the DNA solely depends on the quadruplex topology. The ligands were able to re-orient the 5'-flanking nucleotides in *c-MYC*, but not lateral or diagonal loops present in telomeric DNA topologies. However, it has been reported that strong stabilizing agents like Telomestatin (ΔSASA = 225 $Å^2$) and Naphthalene diimides (ΔSASA = 210 $Å^2$) were able to efficiently re-orient the nucleobases present in the loops of telomeric G-quadruplex structures.[28,36, 67, 82]

MD dynamics and simulations (100 ns) were also extended to rationalize the inability of the ligands to stabilize or induce telomeric parallel topology as evidenced from the CD studies. The final MD snapshot of **Phen-Et** with telomeric parallel G-quadruplex DNA showed that the **Phen-Et** did not stack well on to the G-quartet surface (Figure S23, Supporting Information). Moreover, the *N*-protonated side chains in **Phen-Et** failed to form electrostatic interactions with the backbone of the propeller loop as the distance between them was found to be 10.2 Å, and which led to flexibility of the ligand side chains as evidenced from the RMSD graphs (Figure S24 and S25, Supporting Information). The average RMSD of the loops of parallel quadruplex DNA was around 2.8 Å over 100 ns of MD simulations, which indicated the conformational flexibility of the propeller loops. Furthermore, the two dimensional RMSD map of G-quadruplex – **Phen-Et** complex illustrated the formation of an unstable complex during the MD simulations. Also, the presences of electrostatic and stacking interactions were found to be~ 5 % and ~ 12 % of the 100 ns of the simulation time respectively. The very low prevalence of electrostatic interactions was due to the lengthy (three nucleotides) and flexible propeller loops in the telomeric DNA in comparison to the shorter (one and two nucleotides) and rigid propeller loops in *c-MYC* G-quadruplex DNA. Overall, the data clearly show that the ligand **Phen-Et** forms only

a less stable complex with telomeric parallel G-quadruplex DNA, which accounts for the binding energy of −18.63 ± 3.2 kcal mol^{-1} observed for the complex (Table S7, Supporting Information).

The selectivity of **Phen-Et** and **Phen-Pr** ligands towards G-quadruplex DNAs over dsDNA was also explored by MD simulations. The final MD snapshot of the dsDNA and ligand (Figure S26, Supporting Information), binding energy values (Table 2 and Table S8, Supporting Information), and RMSD graphs (Figure S27, Supporting Information) indicated that ligands have significantly low binding affinity toward dsDNA. Overall, MD simulation studies, SASA analysis, and stacking energy calculations shed lights on how the specificity was achieved by the **Phen-Et** and **Phen-Pr** ligands toward parallel G-quadruplex topology adopted by promoter DNAs.

CONCLUSIONS

We have designed and synthesized bisbenzimidazole carboxamide derivatives of pyridine, 1, 8-naphthyridine and 1,10-phenanthroline to specifically stabilize promoter quadruplexes over telomeric and duplex DNAs. Our studies showed that both aromatic π surface area of the central core and appropriately positioned *N*-alkyl benzimidazole side chains with suitable length of the ligands play a crucial role in discriminating promoter quadruplexes from telomeric DNA. As a result, phenanthroline-based ligands having larger surface area compared to their pyridine and naphthyridine counterparts imparted high specificity toward promoter quadruplexes. Among **Phen-Et** and **Phen-Pr**, the former having ethyl side chain was emerged as the lead compound due to its inability to interact with the loops of telomeric DNA, reflecting in the specific stabilization of promoter quadruplexes (ΔT_m = ~16 - 18°C) over telomeric DNA (ΔT_m = 1 °C). In particular, the ligand has imparted only marginal stability to any of the telomeric DNA topological forms (antiprallel, parallel, hybrid or higher order forms). NMR and CD titration

studies showed that the ligand bound to the *c-MYC* quadruplex via end stacking and upon binding the parallel topology of the *c-MYC* quadruplex was retained. UV-Vis titrations studies further validated the fact that the ligand specifically bound (K_b ~6 x 10^4 M^{-1}) to *c-MYC* quadruplex DNA. Furthermore, *Taq* polymerase stop assay showed that ligand was able to arrest the primer extension (IC_{50} ~1.0 μM) by stabilizing the *c-MYC* quadruplex structure present in the template. Molecular modeling and dynamics studies revealed that the length of the flexible *N,N*-dimethyl aminoethyl side chains present in the ligand was optimal in targeting propeller loops of the *c-MYC* quadruplex to establish electrostatic interactions. In addition, the ligands, by reorienting 5' flanking nucleotides of *c-MYC* quadruplex, maximize the accessible surface area for favorable stacking interactions with the G-quartet of *c-MYC* quadruplex, accounting for the specificity of the ligands toward *c-MYC* quadruplex over telomeric quadruplex structures.

Overall, this study underscores the importance of the flexible side chains in the ligands, which should be taken into consideration for the design of structure-specific quadruplex stabilizing agents. In this context, it should be noted that even when the accurate three dimensional structure of various G-quadruplex DNA topologies are available, right now, there is no well-established methodology to design or identify the structure-specific ligands based on minor structural differences in each quadruplex topologies. Therefore, the benzimidazole scaffolds reported here represent potent and powerful side chains to engineer the quadruplex specific ligands. Systematic explorations and screening of these side chains by attaching with suitable central core having drug-like properties can lead to the evolvement of next generation of ligands, which may find applications in quadruplex DNA based therapeutics. Furthermore, these topology specific ligands could also be utilized along with quadruplex-specific antibodies for the potential applications in visualizing promoter quadruplex DNAs in cellular environment.

SUPPORTING INFORMATION

Experimental procedures, CD melting and titrations curves, UV-Vis absorption spectra, polymerase stop assay, additional results from molecular modeling and dynamics studies and copies of NMR spectra. This material is available free of charge via the Internet at http://pubs.acs.org.

ACKNOWLEDGEMENTS

We are thankful to Professor D. A Case for waiving off the licensing fee for AMBER 12; Dr. S. Srivastava and Ms. M. Joshi, National facility for high-field NMR, TIFR-Mumbai, for their assistance with NMR titrations; Dr. R. Anand for providing access to her laboratory facilities. Computer center, IIT Bombay and NPSF-CDAC, Pune are gratefully acknowledged for providing high performance computing facilities. This work was financially supported by a grant from Department of Atomic Energy-Board of Research in Nuclear Sciences (DAE-BRNS), Government of India (grant no: 2012/37C/4/BRNS-1063). V.D thanks CSIR and IRCC-IIT Bombay and S.H. thanks DAE-BRNS for the fellowships.

DEDICATION

Dedicated to Professor Jyoti Chattopadhyaya on the occasion of his 65th birthday

REFERENCES

[1] Burge, S., Parkinson, G. N., Hazel, P., Todd, A. K., and Neidle, S. (2006) Quadruplex DNA: sequence, topology and structure, *Nucleic Acids Res. 34*, 5402-5415.

[2] Patel, D. J., Phan, A. T., and Kuryavyi, V. (2007) Human telomere, oncogenic promoter and 5'-UTR G-quadruplexes: Diverse higher order DNA and RNA targets for cancer therapeutics, *Nucleic Acids Res. 35*, 7429-7455.

[3] Huppert, J. L., and Balasubramanian, S. (2007) G-quadruplexes in promoters throughout the human genome, *Nucleic Acids Res. 35*, 406-413.

[4] Mukundan, V. T., and Phan, A. T. (2013) Bulges in G-Quadruplexes: Broadening the Definition of G-Quadruplex-Forming Sequences, *J. Am. Chem. Soc. 135*, 5017-5028.

[5] Biffi, G., Tannahill, D., McCafferty, J., and Balasubramanian, S. (2013) Quantitative visualization of DNA G-quadruplex structures in human cells, *Nat. Chem. 5*, 182-186.

[6] Biffi, G., Di Antonio, M., Tannahill, D., and Balasubramanian, S. (2014) Visualization and selective chemical targeting of RNA G-quadruplex structures in the cytoplasm of human cells, *Nat. Chem. 6*, 75-80.

[7] Henderson, A., Wu, Y., Huang, Y. C., Chavez, E. A., Platt, J., Johnson, F. B., Brosh, R. M., Sen, D., and Lansdorp, P. M. (2014) Detection of G-quadruplex DNA in mammalian cells, *Nucleic Acids Res. 42*, 860-869.

[8] Paeschke, K., Bochman, M. L., Garcia, P. D., Cejka, P., Friedman, K. L., Kowalczykowski, S. C., and Zakian, V. A. (2013) Pif1 family helicases suppress genome instability at G-quadruplex motifs, *Nature 497*, 458-462.

[9] Zahler, A. M., Williamson, J. R., Cech, T. R., and Prescott, D. M. (1991) Inhibition of telomerase by G-quartet DMA structures, *Nature 350*, 718-720.

[10] Balasubramanian, S., Hurley, L. H., and Neidle, S. (2011) Targeting G-quadruplexes in gene promoters: a novel anticancer strategy?, *Nat. Rev. Drug Discovery 10*, 261-275.

[11] Kumari, S., Bugaut, A., Huppert, J. L., and Balasubramanian, S. (2007) An RNA G-quadruplex in the 5 ' UTR of the NRAS proto-oncogene modulates translation, *Nat. Chem. Biol. 3*, 218-221.

[12] Arora, A., Dutkiewicz, M., Scaria, V., Hariharan, M., Maiti, S., and Kurreck, J. (2008) Inhibition of translation in living eukaryotic cells by an RNA G-quadruplex motif, *RNA 14*, 1290-1296.

[13] Bidzinska, J., Cimino-Reale, G., Zaffaroni, N., and Folini, M. (2013) G-Quadruplex Structures in the Human Genome as Novel Therapeutic Targets, *Molecules 18*, 12368-12395.

[14] Rodriguez, R., Miller, K. M., Forment, J. V., Bradshaw, C. R., Nikan, M., Britton, S., Oelschlaegel, T., Xhemalce, B., Balasubramanian, S., and Jackson, S. P. (2012) Small-molecule–induced DNA damage identifies alternative DNA structures in human genes, *Nat. Chem. Biol. 8*, 301-310.

[15] Neidle, S. (2010) Human telomeric G-quadruplex: The current status of telomeric G-quadruplexes as therapeutic targets in human cancer, *FEBS J. 277*, 1118-1125.

[16] McLuckie, K. I. E., Di Antonio, M., Zecchini, H., Xian, J., Caldas, C., Krippendorff, B.-F., Tannahill, D., Lowe, C., and Balasubramanian, S. (2013) G-Quadruplex DNA as a Molecular Target for Induced Synthetic Lethality in Cancer Cells, *J. Am. Chem. Soc. 135*, 9640-9643.

[17] Brooks, T. A., Kendrick, S., and Hurley, L. (2010) Making sense of G-quadruplex and i-motif functions in oncogene promoters, *FEBS J. 277*, 3459-3469.

[18] Agarwal, T., Roy, S., Chakraborty, T. K., and Maiti, S. (2010) Selective Targeting of G-Quadruplex Using Furan-Based Cyclic Homooligopeptides: Effect on c-MYC Expression, *Biochemistry 49*, 8388-8397.

[19] Ambrus, A., Chen, D., Dai, J., Jones, R. A., and Yang, D. (2005) Solution Structure of the Biologically Relevant G-Quadruplex Element in the Human c-MYC Promoter. Implications for G-Quadruplex Stabilization, *Biochemistry 44*, 2048-2058.

[20] Phan, A. T., Kuryavyi, V., Burge, S., Neidle, S., and Patel, D. J. (2007) Structure of an unprecedented G-quadruplex scaffold in the human c-kit promoter, *J. Am. Chem. Soc. 129*, 4386-4392.

[21] Hsu, S.-T. D., Varnai, P., Bugaut, A., Reszka, A. P., Neidle, S., and Balasubramanian, S. (2009) A G-Rich Sequence within the c-kit Oncogene Promoter Forms a Parallel G-Quadruplex Having Asymmetric G-Tetrad Dynamics, *J. Am. Chem. Soc. 131*, 13399-13409.

[22] Agrawal, P., Hatzakis, E., Guo, K., Carver, M., and Yang, D. (2013) Solution structure of the major G-quadruplex formed in the human VEGF promoter in K+: insights into loop interactions of the parallel G-quadruplexes, *Nucleic Acids Res. 41*, 10584-10592.

[23] Tong, X., Lan, W., Zhang, X., Wu, H., Liu, M., and Cao, C. (2011) Solution structure of all parallel G-quadruplex formed by the oncogene RET promoter sequence, *Nucleic Acids Res. 39*, 6753-6763.

[24] De Armond, R., Wood, S., Sun, D. Y., Hurley, L. H., and Ebbinghaus, S. W. (2005) Evidence for the presence of a guanine quadruplex forming region within a polypurine tract of the hypoxia inducible factor 1 alpha promoter, *Biochemistry 44*, 16341-16350.

[25] Buscaglia, R., Miller, M. C., Dean, W. L., Gray, R. D., Lane, A. N., Trent, J. O., and Chaires, J. B. (2013) Polyethylene glycol binding alters human telomere G-quadruplex structure by conformational selection, *Nucleic Acids Res. 41*, 7934-7946.

[26] Hänsel, R., Löhr, F., Trantirek, L., and Dötsch, V. (2013) High-Resolution Insight into G-Overhang Architecture, *J. Am. Chem. Soc. 135*, 2816-2824.

[27] Haensel, R., Loehr, F., Foldynova-Trantirkova, S., Bamberg, E., Trantirek, L., and Doetsch, V. (2011) The parallel G-quadruplex structure of vertebrate telomeric repeat sequences is not the preferred folding topology under physiological conditions, *Nucleic Acids Res. 39*, 5768-5775.

[28] Luu, K. N., Phan, A. T., Kuryavyi, V., Lacroix, L., and Patel, D. J. (2006) Structure of the human telomere in K+ solution: An intramolecular (3+1) G-quadruplex scaffold, *J. Am. Chem. Soc. 128*, 9963-9970.

[29] Phan, A. T., Kuryavyi, V., Luu, K. N., and Patel, D. J. (2007) Structure of two intramolecular G-quadruplexes formed by natural human telomere sequences in K+ solution, *Nucleic Acids Res. 35*, 6517-6525.

[30] Petraccone, L., Spink, C., Trent, J. O., Garbett, N. C., Mekmaysy, C. S., Giancola, C., and Chaires, J. B. (2011) Structure and Stability of Higher-Order Human Telomeric Quadruplexes, *J. Am. Chem. Soc. 133*, 20951-20961.

[31] Luedtke, N. W. (2009) Targeting G-Quadruplex DNA with Small Molecules, *Chimia 63*, 134-139.

[32] Ou, T.-m., Lu, Y.-j., Tan, J.-h., Huang, Z.-s., Wong, K.-Y., and Gu, L.-q. (2008) G-quadruplexes: Targets in anticancer drug design, *Chemmedchem 3*, 690-713.

[33] Mohanty, J., Barooah, N., Dhamodharan, V., Harikrishna, S., Pradeepkumar, P. I., and Bhasikuttan, A. C. (2013) Thioflavin T as an Efficient Inducer and Selective Fluorescent Sensor for the Human Telomeric G-Quadruplex DNA, *J. Am. Chem. Soc. 135*, 367-376.

[34] Webba da Silva, M. (2007) Geometric Formalism for DNA Quadruplex Folding, *Chem. Eur. J. 13*, 9738-9745.

[35] Campbell, N. H., Patel, M., Tofa, A. B., Ghosh, R., Parkinson, G. N., and Neidle, S. (2009) Selectivity in Ligand Recognition of G-Quadruplex Loops, *Biochemistry 48*, 1675-1680.

[36] Haider, S. M., Neidle, S., and Parkinson, G. N. (2011) A structural analysis of G-quadruplex/ligand interactions, *Biochimie 93*, 1239-1251.

[37] Xue, L., Ranjan, N., and Arya, D. P. (2011) Synthesis and Spectroscopic Studies of the Aminoglycoside (Neomycin)-Perylene Conjugate Binding to Human Telomeric DNA, *Biochemistry 50*, 2838-2849.

[38] Sparapani, S., Haider, S. M., Doria, F., Gunaratnam, M., and Neidle, S. (2010) Rational Design of Acridine-Based Ligands with Selectivity for Human Telomeric Quadruplexes, *J. Am. Chem. Soc. 132*, 12263-12272.

[39] Di Leva, F. S., Zizza, P., Cingolani, C., D'Angelo, C., Pagano, B., Amato, J., Salvati, E., Sissi, C., Pinato, O., Marinelli, L., Cavalli, A., Cosconati, S., Novellino, E., Randazzo, A., and Biroccio, A. (2013) Exploring the Chemical Space of G-Quadruplex Binders: Discovery of a Novel Chemotype Targeting the Human Telomeric Sequence, *J. Med. Chem. 56*, 9646-9654.

[40] Hamon, F., Largy, E., Guédin-Beaurepaire, A., Rouchon-Dagois, M., Sidibe, A., Monchaud, D., Mergny, J.-L., Riou, J.-F., Nguyen, C.-H., and Teulade-Fichou, M.-P. (2011) An Acyclic Oligoheteroaryle That Discriminates Strongly between Diverse G-Quadruplex Topologies, *Angew. Chem., Int. Ed. 50*, 8745-8749.

[41] Nicoludis, J. M., Miller, S. T., Jeffrey, P. D., Barrett, S. P., Rablen, P. R., Lawton, T. J., and Yatsunyk, L. A. (2012) Optimized End-Stacking Provides Specificity of N-Methyl Mesoporphyrin IX for Human Telomeric G-Quadruplex DNA, *J. Am. Chem. Soc. 134*, 20446-20456.

[42] Di Antonio, M., Biffi, G., Mariani, A., Raiber, E.-A., Rodriguez, R., and Balasubramanian, S. (2012) Selective RNA Versus DNA G-Quadruplex Targeting by In Situ Click Chemistry, *Angew. Chem., Int. Ed. 51*, 11073-11078.

[43] Seenisamy, J., Bashyam, S., Gokhale, V., Vankayalapati, H., Sun, D., Siddiqui-Jain, A., Streiner, N., Shin-ya, K., White, E., Wilson, W. D., and Hurley, L. H. (2005) Design and Synthesis of an Expanded Porphyrin That Has Selectivity for the c-MYC G-Quadruplex Structure, *J. Am. Chem. Soc. 127*, 2944-2959.

[44] Jantos, K., Rodriguez, R., Ladame, S., Shirude, P. S., and Balasubramanian, S. (2006) Oxazole-Based Peptide Macrocycles: A New Class of G-Quadruplex Binding Ligands, *J. Am. Chem. Soc. 128*, 13662-13663.

[45] McLuckie, K. I. E., Waller, Z. A. E., Sanders, D. A., Alves, D., Rodriguez, R., Dash, J., McKenzie, G. J., Venkitaraman, A. R., and Balasubramanian, S. (2011) G-Quadruplex-Binding Benzo[a]phenoxazines Down-Regulate c-KIT Expression in Human Gastric Carcinoma Cells, *J. Am. Chem. Soc. 133*, 2658-2663.

[46] Bejugam, M., Sewitz, S., Shirude, P. S., Rodriguez, R., Shahid, R., and Balasubramanian, S. (2007) Trisubstituted Isoalloxazines as a New Class of G-Quadruplex Binding Ligands: Small Molecule Regulation of c-kit Oncogene Expression, *J. Am. Chem. Soc. 129*, 12926-12927.

[47] Chauhan, A., Paladhi, S., Debnath, M., Mandal, S., Das, R. N., Bhowmik, S., and Dash, J. (2014) A small molecule peptidomimetic that binds to c-KIT1 G-quadruplex and exhibits antiproliferative properties in cancer cells, *Bioorg. Med. Chem. 22*, 4422-4429.

[48] Jain, A. K., and Bhattacharya, S. (2011) Interaction of G-Quadruplexes with Nonintercalating Duplex-DNA Minor Groove Binding Ligands, *Bioconjugate Chem. 22*, 2355-2368.

[49] Bhattacharya, S., Chaudhuri, P., Jain, A. K., and Paul, A. (2010) Symmetrical Bisbenzimidazoles with Benzenediyl Spacer: The Role of the Shape of the Ligand on the Stabilization and Structural Alterations in Telomeric G-Quadruplex DNA and Telomerase Inhibition, *Bioconjugate Chem. 21*, 1148-1159.

[50] Jain, A. K., Paul, A., Maji, B., Muniyappa, K., and Bhattacharya, S. (2012) Dimeric 1,3-Phenylene-bis(piperazinyl benzimidazole)s: Synthesis and Structure–Activity Investigations on their Binding with Human Telomeric G-Quadruplex DNA and Telomerase Inhibition Properties, *J. Med. Chem. 55*, 2981-2993.

[51] Wang, P., Leung, C.-H., Ma, D.-L., Yan, S.-C., and Che, C.-M. (2010) Structure-Based Design of Platinum(II) Complexes as c-myc Oncogene Down-Regulators and Luminescent Probes for G-Quadruplex DNA, *Chem. Eur. J. 16*, 6900-6911.

[52] Largy, E., Hamon, F., Rosu, F., Gabelica, V., De Pauw, E., Guédin, A., Mergny, J.-L., and Teulade-Fichou, M.-P. (2011) Tridentate N-Donor Palladium(II) Complexes as Efficient Coordinating Quadruplex DNA Binders, *Chem. Eur. J. 17*, 13274-13283.

[53] Li, G., Huang, J., Zhang, M., Zhou, Y., Zhang, D., Wu, Z., Wang, S., Weng, X., Zhou, X., and Yang, G. (2008) Bis(benzimidazole)pyridine derivative as a new class of G-quadruplex inducing and stabilizing ligand, *Chem. Commun.*, 4564-4566.

[54] Pennarun, G., Granotier, C., Gauthier, L. R., Gomez, D., and Boussin, F. D. (2005) Apoptosis related to telomere instability and cell cycle alterations in human glioma cells treated by new highly selective G-quadruplex ligands, *Oncogene 24*, 2917-2928.

[55] Dhamodharan, V., Harikrishna, S., Jagadeeswaran, C., Halder, K., and Pradeepkumar, P. I. (2012) Selective G-quadruplex DNA Stabilizing Agents Based on Bisquinolinium and Bispyridinium Derivatives of 1,8-Naphthyridine, *J. Org. Chem. 77*, 229-242.

[56] De Cian, A., DeLemos, E., Mergny, J.-L., Teulade-Fichou, M.-P., and Monchaud, D. (2007) Highly Efficient G-Quadruplex Recognition by Bisquinolinium Compounds, *J. Am. Chem. Soc. 129*, 1856-1857.

[57] Larsen, A. F., Nielsen, M. C., and Ulven, T. (2012) Tetrasubstituted Phenanthrolines as Highly Potent, Water-Soluble, and Selective G-Quadruplex Ligands, *Chem. Eur. J. 18*, 10892-10902.

[58] Gracie, K., Dhamodharan, V., Pradeepkumar, P. I., Faulds, K., and Graham, D. (2014) Qualitative SERS analysis of G-quadruplex DNAs using selective stabilising ligands, *Analyst 139*, 4458-4465.

[59] Monchaud, D., Yang, P., Lacroix, L., Teulade-Fichou, M.-P., and Mergny, J.-L. (2008) A metal-mediated conformational switch controls G-quadruplex binding affinity, *Angew. Chem., Int. Ed. 47*, 4858-4861.

[60] Seth, P. P., Robinson, D. E., Jefferson, E. A., and Swayze, E. E. (2002) Efficient solution phase synthesis of 2-(N-acyl)-aminobenzimidazoles, *Tetrahedron Letters 43*, 7303-7306.

[61] Guédin, A., Lacroix, L., and Mergny, J.-L. (2010) Thermal Melting Studies of Ligand DNA Interactions, In *Drug-DNA Interaction Protocols* (Fox, K. R., Ed.), pp 25-35, Humana Press.

[62] Xue, Y., Kan, Z.-y., Wang, Q., Yao, Y., Liu, J., Hao, Y.-h., and Tan, Z. (2007) Human Telomeric DNA Forms Parallel-Stranded Intramolecular G-Quadruplex in K+ Solution under Molecular Crowding Condition, *J. Am. Chem. Soc. 129*, 11185-11191.

[63] Singh, V., Azarkh, M., Drescher, M., and Hartig, J. S. (2012) Conformations of individual quadruplex units studied in the context of extended human telomeric DNA, *Chem. Commun. 48*, 8258-8260.

[64] Rezler, E. M., Seenisamy, J., Bashyam, S., Kim, M. Y., White, E., Wilson, W. D., and Hurley, L. H. (2005) Telomestatin and diseleno sapphyrin bind selectively to two different forms of the human telomeric G-quadruplex structure, *J. Am. Chem. Soc. 127*, 9439-9447.

[65] Dash, J., Shirude, P. S., Hsu, S.-T. D., and Balasubramanian, S. (2008) Diarylethynyl Amides That Recognize the Parallel Conformation of Genomic Promoter DNA G-Quadruplexes, *J. Am. Chem. Soc. 130*, 15950-15956.

[66] Dai, J., Carver, M., Hurley, L. H., and Yang, D. (2011) Solution Structure of a 2:1 Quindoline–c-MYC G-Quadruplex: Insights into G-Quadruplex-Interactive Small Molecule Drug Design, *J. Am. Chem. Soc. 133*, 17673-17680.

[67] Chung, W. J., Heddi, B., Tera, M., Iida, K., Nagasawa, K., and Phan, A. T. (2013) Solution Structure of an Intramolecular (3 + 1) Human Telomeric G-Quadruplex Bound to a Telomestatin Derivative, *J. Am. Chem. Soc. 135*, 13495-13501.

[68] Chung, W. J., Heddi, B., Hamon, F., Teulade-Fichou, M.-P., and Phan, A. T. (2014) Solution Structure of a G-quadruplex Bound to the Bisquinolinium Compound Phen-DC3, *Angew. Chem., Int. Ed. 53*, 999-1002.

[69] Ma, D.-L., Chan, D. S.-H., Fu, W.-C., He, H.-Z., Yang, H., Yan, S.-C., and Leung, C.-H. (2012) Discovery of a Natural Product-Like c-*myc* G-Quadruplex DNA Groove-Binder by Molecular Docking, *PLoS ONE 7*, e43278.

[70] Yaku, H., Murashima, T., Miyoshi, D., and Sugimoto, N. (2010) Anionic phthalocyanines targeting G-quadruplexes and inhibiting telomerase activity in the presence of excessive DNA duplexes, *Chem. Commun. 46*, 5740-5742.

[71] Kieltyka, R., Englebienne, P., Moitessier, N., and Sleiman, H. (2010) Quantifying Interactions Between G-Quadruplex DNA and Transition-Metal Complexes, In *G-Quadruplex DNA* (Baumann, P., Ed.), pp 223-255, Humana Press.

[72] Koirala, D., Dhakal, S., Ashbridge, B., Sannohe, Y., Rodriguez, R., Sugiyama, H., Balasubramanian, S., and Mao, H. (2011) A single-molecule platform for investigation of interactions between G-quadruplexes and small-molecule ligands, *Nat. Chem. 3*, 782-787.

[73] Han, H., Hurley, L. H., and Salazar, M. (1999) A DNA polymerase stop assay for G-quadruplex-interactive compounds, *Nucleic Acids Res. 27*, 537-542.

[74] Sun, D., and Hurley, L. (2010) Biochemical Techniques for the Characterization of G-Quadruplex Structures: EMSA, DMS Footprinting, and DNA Polymerase Stop Assay, In *G-Quadruplex DNA* (Baumann, P., Ed.), pp 65-79, Humana Press.

[75] Frisch, M., Trucks, G. W., Schlegel, H. B., Scuseria, G. E., Robb, M. A., Cheeseman, J. R., Scalmani, G., Barone, V., Mennucci, B., and Petersson, G. A. (2009) Gaussian 09, Revision A. 02, Gaussian, *Inc., Wallingford, CT 200*.

[76] Parkinson, G. N., Lee, M. P. H., and Neidle, S. (2002) Crystal structure of parallel quadruplexes from human telomeric DNA, *Nature 417*, 876-880.

[77] Wang, Y., and Patel, D. J. (1993) Solution structure of the human telomeric repeat d[AG3(T2AG3)3] G-tetraplex, *Structure 1*, 263-282.

[78] Case, D., Darden, T., Cheatham III, T., Simmerling, C., Wang, J., Duke, R., Luo, R., Walker, R., Zhang, W., and Merz, K. (2012) AMBER 12, *University of California, San Francisco*.

[79] Wang, J. M., Wolf, R. M., Caldwell, J. W., Kollman, P. A., and Case, D. A. (2004) Development and testing of a general amber force field, *J. Comput. Chem. 25*, 1157-1174.

[80] Kollman, P. A., Massova, I., Reyes, C., Kuhn, B., Huo, S. H., Chong, L., Lee, M., Lee, T., Duan, Y., Wang, W., Donini, O., Cieplak, P., Srinivasan, J., Case, D. A., and Cheatham, T. E. (2000) Calculating structures and free energies of complex molecules: Combining molecular mechanics and continuum models, *Acc. Chem. Res. 33*, 889-897.

[81] Lech, C. J., Heddi, B., and Phan, A. T. (2013) Guanine base stacking in G-quadruplex nucleic acids, *Nucleic Acids Res. 41*, 2034-2046.

[82] Haider, S. M., Autiero, I., and Neidle, S. (2011) Surface area accessibility and the preferred topology of telomeric DNA quadruplex–ligand complexes, *Biochimie 93*, 1275-1279.

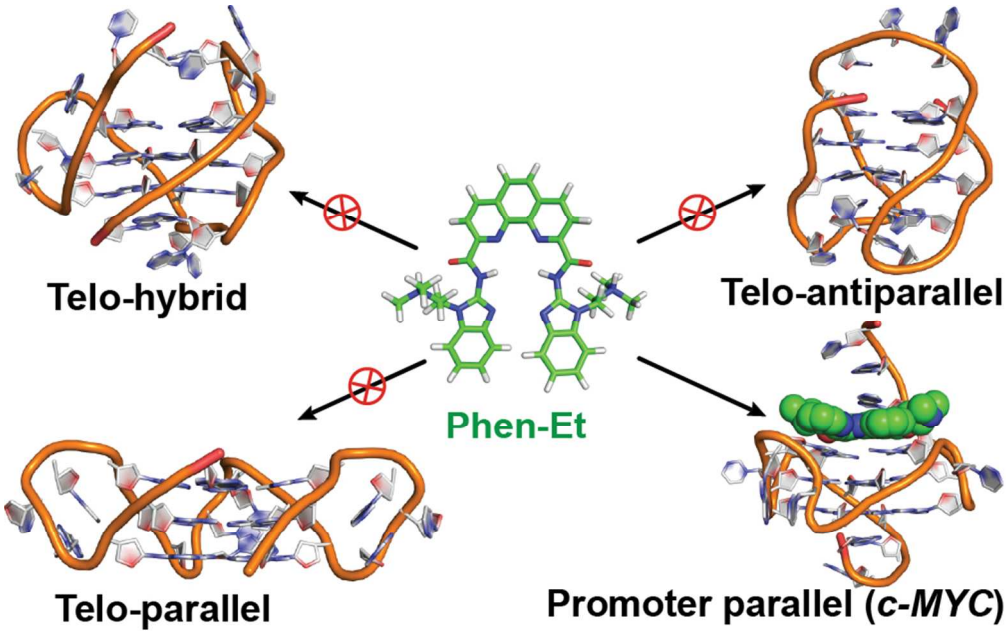

85x53mm (300 x 300 DPI)